



Influence of surface structure on the performance of mono-like Si PERC solar cell

Rui Tong^a, Weipeng Zhang^b, Ximan Ke^b, Dongming Liu^{a,*}, Zhongwei Zhang^b

^a School of Materials Science and Engineering, Anhui University of Technology, Maanshan, Anhui, 243002, PR China
^b Nantong Sumin Renewable Energy Technology Co., Ltd, Nantong, Jiangsu, 226333, PR China

ARTICLE INFO

Keywords:

Mono-like Si
Solar cell
Texturing
Surface structure
Efficiency

ABSTRACT

Mono-like Si wafers were textured by both alkaline solution and metal-assisted chemical etching (MACE) process. The influences of surface textures on the diffusion process, surface passivation, electrical property and performance of solar cells were investigated. The results show that the pyramid-like structures obtained by alkaline texturing facilitates a higher surface doping concentration, larger junction depth after diffusion and better passivation effect, compared with the honeycomb-like structures generated by MACE texturing. In the same wafer textured by alkaline solution or MACE, the mono-crystalline region exhibits a higher quantum efficiency than the multi-crystalline region. By combining the MACE and alkaline texturing processes, the honeycomb- and pyramid-like structures were generated on the surface of mono-like Si wafer, resulting in a conversion efficiency of 21.39% that is higher than that of the individually MACE or alkaline-textured solar cells by 0.4% and 0.02%, respectively.

1. Introduction

In recent years, with the continued development of photovoltaic technologies, mono- and multi-crystalline Si solar cells have occupied more than 90% of the market share [1]. However, the traditional multi-crystalline Si wafer is no longer compatible with passivated emitter and rear cell (PERC) technology due to its higher concentration of grain boundaries, dislocations and metal impurities as compared with mono-crystalline Si wafer [2]. The casting technology used for producing mono-like Si wafer becomes the research focus in the industry again, as the mono-like crystalline cell shows comparable performance with mono-crystalline counterpart and manufacturing cost close to multi-crystalline cell. However, in contrast with the traditional Czochralski mono-crystalline Si wafer, there is still a small fraction of multi-crystalline regions with relative small grain size distributed within the casting block [3,4]. Therefore, the multi-crystalline regions always coexist with mono-crystalline regions within a single wafer [5]. In recent years, there have been constant efforts to further improve both the quality of mono-like Si wafer [6,7] and the conversion efficiency of mono-like Si solar cell [8,9].

In the industrial manufacturing process of crystalline Si solar cell, texturing is a key step with the main purpose to increase the light

absorption via the change of surface structures. For instance, the inverted nanoparamids can be generated on the wafer surface by interference lithography followed by KOH etching and metal (Ag nanoparticles) assisted etching [10,11]. On the other hand, laser texturing combined post-texturing cleanings and reactive ion etching (RIE) texturing combined chemical texturing by alkaline solution can generate quite different surface structures [12,13]. Currently, the texturing processes that are scalable for industrial use with acceptable cost include acid texturing by HF/HNO₃/H₂O mixed solution, MACE and alkaline (mainly uses KOH or NaOH solution) texturing. Acid texturing [14,15] and MACE texturing [16,17] are mainly used for multi-crystalline Si wafer, while alkaline texturing is primarily developed for mono-crystalline Si wafer [18]. Recently, Gao et al. used MACE and alkali anisotropic etching technique to fabricate an inverted pyramid structure on mono-crystalline Si. The efficiency of 21.4% was obtained for the Si PERC solar cell from the wafer etched for 30 s [19].

For the fabrication of mono-like Si solar cell, either MACE or alkaline texturing is currently used, and the surface structures produced by these two processes are quite different. In the mono-crystalline region, alkaline texturing leads to the formation of pyramid-like structure, while honeycomb structure is formed after MACE texturing. The benefit of using MACE texturing is the lower reflectivity in the multi-crystalline

* Corresponding author.

E-mail address: ldm_ahut@163.com (D. Liu).



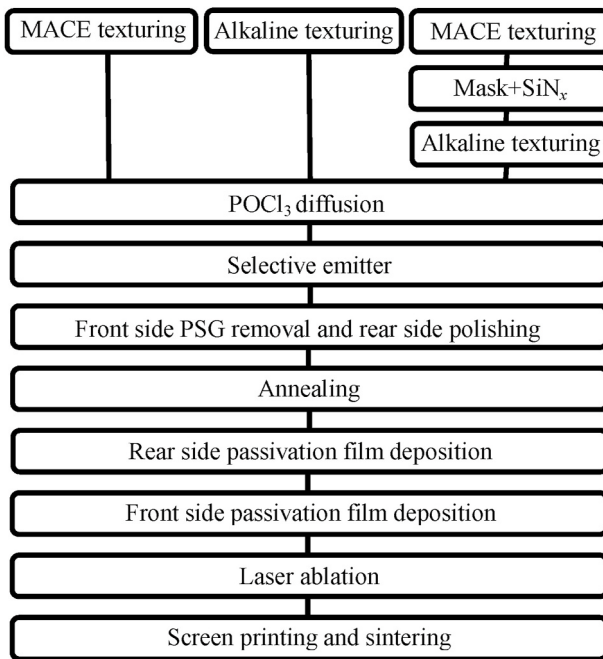


Fig. 1. Experimental design and flow chart for the fabrication of PERC solar cells based on mono-like Si wafers.

region, while after alkaline texturing lower reflectivity is obtained in the mono-crystalline region. However, for the mono-like Si wafer with both mono- and multi-crystalline regions, the performance of solar cell is difficult to be improved by using a single texturing method, and the impact of different texture structures on the cell performance still needs to be examined to confirm whether there is a better way to improve the conversion efficiency.

In this paper, a batch of mono-like Si wafers with both mono- and multi-crystalline structures were used for the fabrication of cells. We analyzed the effects of alkaline and MACE texturing on the surface structure and performance of the solar cells. Based on our results, we developed a SiN_x mask method that allowed for selective alkaline texturing in the mono-crystalline region and MACE texturing in the multi-crystalline region. The use of these selective etching process resulted in the enhancement of efficiency and possible mechanisms were discussed.

2. Experimental

2.1. Sample preparation

The substrate used in this work is P-type mono-like Si wafers (158.75 mm × 158.75 mm) with a thickness of 180 μm and resistivity of 0.5–1.5 Ω cm. These wafers were cut from the same ingot and therefore have the same structure. Based on the calculation by OpenCV, the multi-crystalline and mono-crystalline regions account for about 2% and 98% of the total area, respectively. Before the texturing process, all the wafers were etched by KOH solution to decrease the impact of saw damage layer [20]. The wafers are divided into groups A, B and C, which were textured respectively by alkaline solution, MACE process and the combined process (alkaline + MACE texturing). For alkaline texturing process (group A), the wafers were etched by KOH solution containing commercial texturing additives, and then washed by KOH solution, HF/HCl/H₂O mixed solution and finally by de-ionized water. Group B of wafers were textured by the MACE process, which has been detailed elsewhere [21]. For group C, the alkaline and MACE texturing were combined. In a typical process, the MACE texturing was applied to the wafers and the multi-crystalline region was masked by a SiN_x layer, then

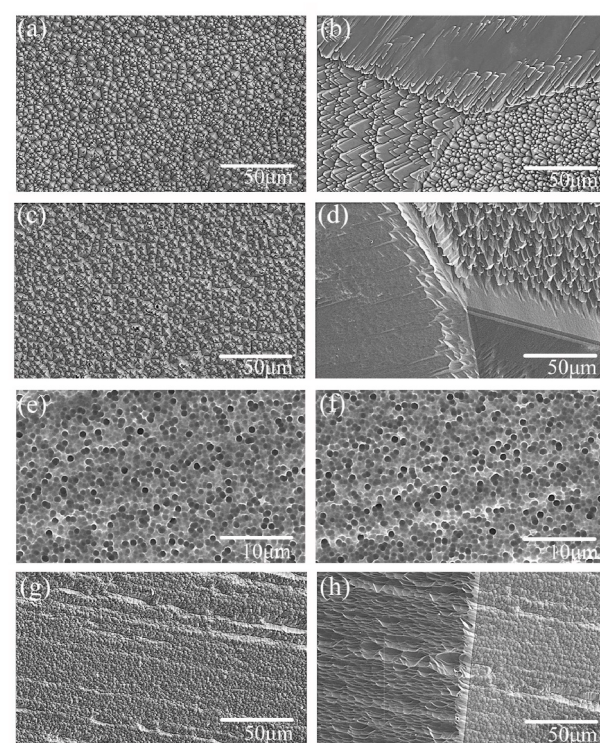


Fig. 2. SEM images of mono-like Si wafers after different texturing process and polishing: (a) mono-crystalline region after alkaline texturing; (b) multi-crystalline region after alkaline texturing; (c) mono-crystalline region after alkaline texturing and acid polishing (HF/HNO₃/H₂O); (d) multi-crystalline region after alkaline texturing and acid polishing; (e) mono-crystalline region after MACE texturing; (f) multi-crystalline region after MACE texturing; (g) mono-crystalline region after MACE texturing and acid polishing; (h) multi-crystalline region after MACE texturing and acid polishing.

the alkaline texturing was performed and the resultant wafers were finally washed by the same procedure as group A. Afterwards, a standard process was carried out to fabricate the cell, which includes the processes of low pressure diffusion, selective emitter (SE) process, front side phosphosilicate glass (PSG) removal and rear side polishing, oxidation, backside passivation, front surface coating, backside laser grooving, printing and sintering (see Fig. 1).

In the following text, we mark the different samples with the process name and mono-/multi crystalline region. For example, the mono-crystalline region of wafer from group A is labeled as “Alkaline-mono”, and the label “MACE-multi-polishing” means the multi-crystalline region of a sample that was proceeded after MACE texturing and polishing.

2.2. Characterizations

Surface morphology was observed with a Hitachi SU3500 scanning electron microscope (SEM). Reflectivity, external and internal quantum efficiency (EQE and IQE) were measured by using a QE system (Pte, PVE300-IVT) in a wavelength range from 300 to 1100 nm. The diffusion depth and concentration of phosphorus atoms in the Si wafer were evaluated by using electrochemical capacitance-voltage (ECV) profiling (WEP, CVP21). The sheet resistance was measured by using the four-probe method (NAPSON, RG-200PV*DF-9P). The minority carrier lifetime of the textured Si wafer was measured by a Sinton WCT-120 system based on the quasi-steady-state photo conductance method. The electrical performance of the solar cells was characterized by a HALM cetisPV-IUCT-2400 I-V tester under AM1.5G.

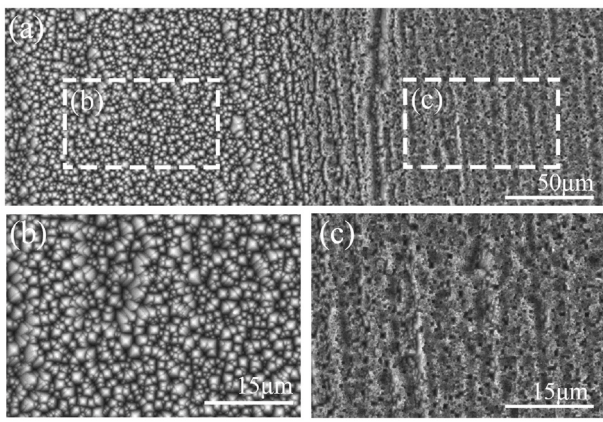


Fig. 3. SEM images of mono-like Si wafer after MACE and alkaline texturing with mask: (a) the intersection of two different surface structures; (b) enlarged view of area b in Fig. 3a; (c) enlarged view of area c in Fig. 3a.

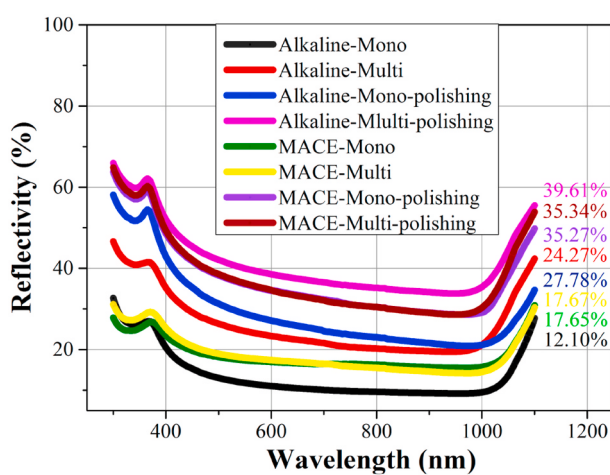


Fig. 4. Surface reflectivity of different wafers.

3. Results and discussion

In the present work, we compare the influence of texturing methods on the surface structure, reflectivity, diffusion depth and surface concentration, sheet resistance, QE and performance of the fabricated mono-like Si solar cells. The alkaline texturing process usually results in the formation of anisotropic structures that are dependent on the orientations of the crystalline grains, while the typical texture structures are isotropic for the MACE process. Fig. 2 and Fig. 3 show the SEM images of the surface for Si wafers after texturing by different processes. For the alkaline-textured wafers, the mono-crystalline region shows pyramid-like structures, while the multi-crystalline regions are dominated by tilted pyramids and laminated structures and the grain boundaries can be seen clearly. The formation of these structures strongly reduces the surface reflectivity depending upon the surface structures. For the wafers after MACE texturing, the mono-crystalline and multi-crystalline regions show the same honeycomb-like surface structures with a hole diameter between 500 and 700 nm. The formation of nanoscale porosity strongly reduces the reflectivity to around 18%. After polishing with the HF/HNO₃/H₂O mixed solution (etching depth is about 3.5 μm), a notable rise of reflectivity is observed as the surface becomes rather smooth, as shown in Fig. 4. From the SEM images shown in Fig. 2, the shape of the previous pyramidal textures remains almost unaffected after polishing for the alkaline texturing samples, while the honeycomb-like structures almost disappear completely for the MACE processed wafers, and the corroded Si substrate can be observed clearly

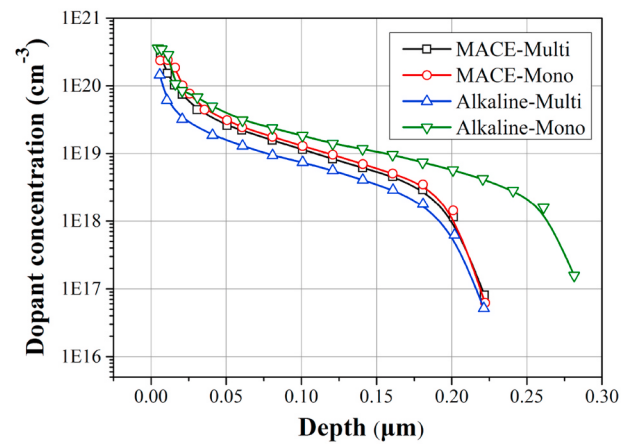


Fig. 5. ECV profiles of different wafers.

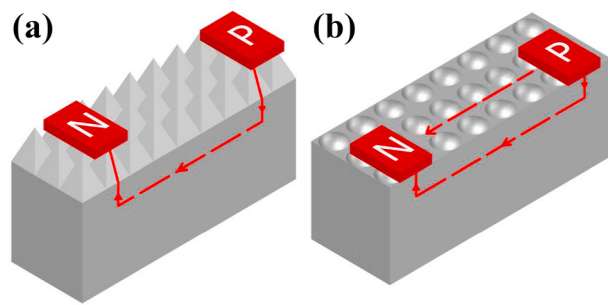


Fig. 6. Electron transport pathways on the surfaces after (a) alkaline and (b) MACE texturing.

for both mono-crystalline and multi-crystalline regions. For the wafers after texturing by both MACE and alkaline solution (see experimental section for details), both pyramid-like and honeycomb-like structures are presented on the wafer surface (see Fig. 3). In addition, the reflectivity in the pyramid (or honeycomb) regions are close to the same region textured by only alkaline solution (or MACE process), indicating the strong dependence of optical properties on surface structures.

It has been well established that the doping concentration and diffusion depth of the dopant are strongly correlated with the surface structures, and surfaces with sharp structures with a high aspect ratio favors a larger surface doping concentration and junction depth [22]. In order to verify the effect of texturing methods on the diffusion surface concentration and junction depth, the Si wafers textured by alkaline solution and MACE process were diffused in the same tube furnace at 820 °C for 85 min. The sheet resistance and ECV curve of different regions for the different Si wafers were then measured. As shown in Fig. 5, for the MACE-textured wafers, there is little difference in the diffusion concentration and junction depth between the mono-crystalline region and the multi-crystalline region, which may be correlated to the similar surface textures. For the alkaline-textured wafers, the mono-crystalline regions show a higher surface concentration and a larger diffusion depth compared with the MACE-textured wafers. Furthermore, the sheet resistances of the mono-crystalline region after alkaline and MACE texturing are 130 Ω/□ and 110 Ω/□, respectively. It is generally believed that the higher resistance value is associated with a lower surface doping concentration and a shallower junction depth [23,24]. However, considering that the resistance is also dependent on the surface structures of the wafer, the higher doping concentration in a low reflectivity surfaces (e.g. for the alkaline-textured samples) do not necessarily result in a lower resistance. In the present case, the alkaline-textured wafers are covered by a layer of pyramid-like structures, while the MACE-textured wafers are dominated by the

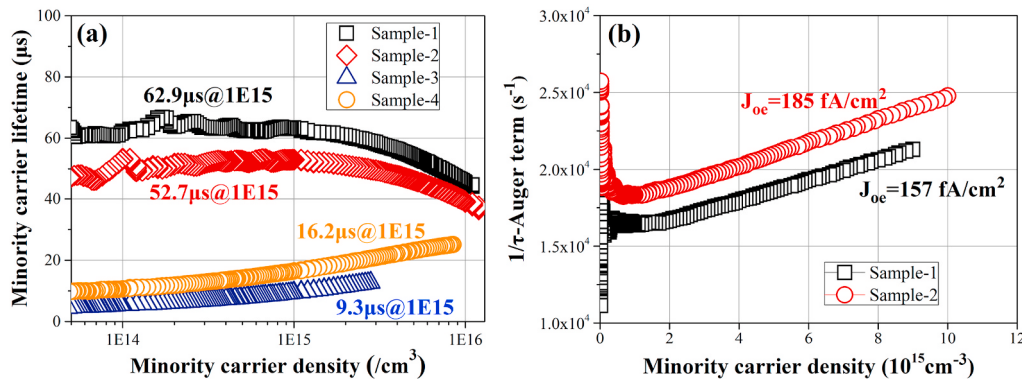


Fig. 7. (a) Minority carrier lifetime and (b) Auger-corrected inverse lifetime as a function of injection level.

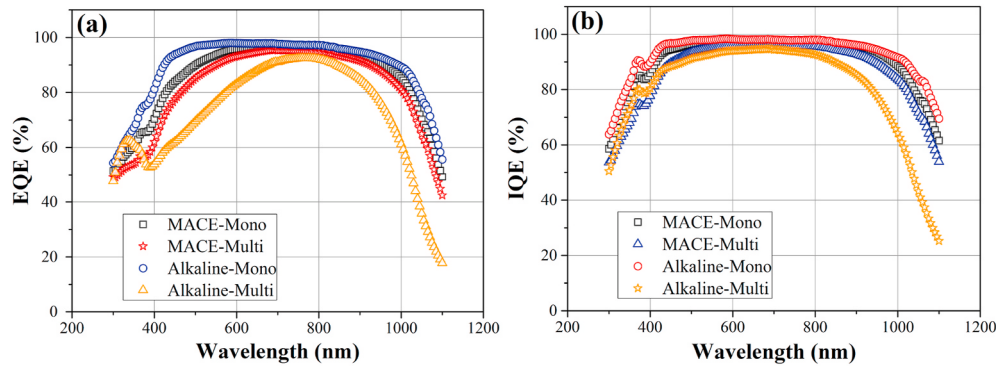


Fig. 8. (a) EQE and (b) IQE curves of the 158.75 mm × 158.75 mm cells.

honeycomb-like surface structures. During the sheet resistance testing, the path and distance of current transmission will be different (see Fig. 6), and this difference explains the relation between sheet resistance and surface structures.

In order to further study the correlation between minority carrier lifetime, saturation current density and surface morphology, we examined four samples that were fabricated under different conditions. Sample-1 was subjected to alkaline texturing, and sample-2 to MACE texturing. Then the textured wafers were subjected to double-sided diffusion, PSG removal and double-sided SiN_x passivation treatment. For sample-3 and sample-4, alkaline and MACE texturing were applied, respectively. The textured wafers were then processed by double-sided acid polishing and Al₂O₃ + SiN_x stack layers passivation on both sides. In these experiments, the HF/HNO₃/H₂O mixed solution was used for polishing, and the etching depth was 3.5 μm.

Fig. 7 gives the minority carrier lifetime and emitter saturation current density (J_{oe}) of samples (measured in the mono-crystalline

region) textured by different processes. It is observed from Fig. 7a that the minority carrier lifetimes of the samples textured by alkaline solution (sample-1) and MACE (sample-2) are 62.9 and 52.7 μs, respectively. In addition, Fig. 7b shows that sample-1 has a lower saturation current density as compared to sample-2. We believe that it is related to the disordered sub-nanometer honeycomb structures of the surface generated by the MACE process, the complex surface structures result in lower minority life and higher J_{oe} . Sample-3 and sample-4 that were polished by acid solution have the minority lifetimes of 9.3 and 16.2 μs, respectively. From the previous SEM images and reflectivity analysis, the pyramid-like structures cannot be completely removed after polishing and thus the reflectivity changes slightly to 27.78%. In comparison, the sub-nano porous structures of the MACE-textured samples disappeared completely, leading to a notable increase of reflectivity to more than 35% that facilitates passivation by Al₂O₃+SiN_x stack layers.

Due to the presence of larger amount of dislocations, grain boundaries and impurities, the rates of SRH (Shockley-Read-Hall)

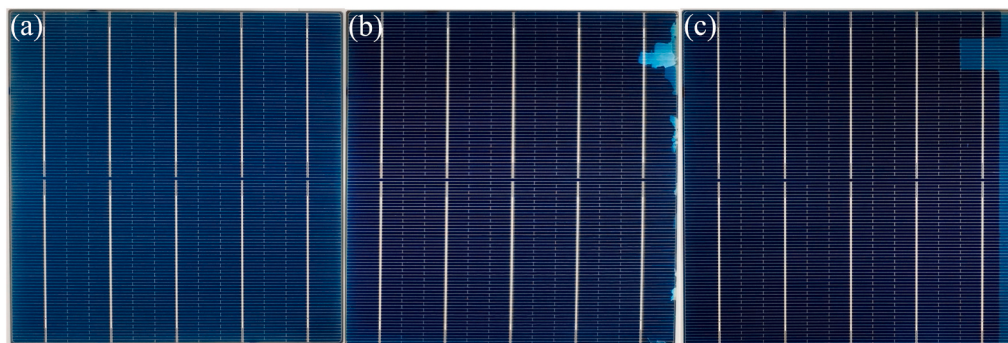


Fig. 9. Photographs of the 158.75 mm × 158.75 mm mono-like Si solar cells textured by (a) MACE, (b) alkaline solution and (c) MACE + alkaline solution.

Table 1

Electrical parameters of the 158.75 mm × 158.75 mm solar cells.

Texturing	Efficiency (%)	V _{oc} (V)	J _{sc} (mA/cm ²)	FF (%)
MACE	20.99	0.667	39.99	78.68
Alkaline	21.37	0.670	40.08	79.58
MACE + alkaline	21.39	0.670	40.17	79.46

recombination and Auger recombination are much higher in multi-crystalline wafers as compared with the mono-crystalline counterparts. For the solar cell based on alkaline-textured wafer, we found that the mono-crystalline region shows higher EQE and IQE than those of the multi-crystalline region (see Fig. 8), which can be primarily attributed to the difference in surface reflectivity. In addition, the low EQE and IQE in the medium and long wavelength regions can be partially related to the faster carrier recombination mediated by defects in the multi-crystalline region. For the cell constructed by MACE-textured wafer, both IQE and EQE recorded for the multi-crystalline region are lower than those of the mono-crystalline region, which can be again rationalized by the difference in the recombination rate in different regions.

Fig. 9 shows the photographs of the solar cell based on mono-like Si wafer textured by different processes. According to a standard measurement, the conversion efficiencies of the cells based on alkaline-textured and MACE-textured wafers are 21.37% and 20.99%, respectively. As the multi-crystalline area only accounts for about 2% of the entire Si wafer, the average reflectivity of the cell using the alkaline-textured wafer is much lower than that of the cell using the MACE-textured wafer, which results in a higher short-circuit current density (J_{sc}) of the solar cell. For the solar cell made from wafer textured by a combination of MACE and alkaline solution, the measured efficiency is 21.39%, which is slightly higher than that of the alkaline-textured cell. Compared with the cell based on MACE texturing, the one based on alkaline and MACE + alkaline texturing have better open circuit voltage (V_{oc}) because of the good surface passivation quality, and for the MACE-textured sample, the fill factor (FF) is worse because the surface structures are disordered, which may cause the bad passivation and contact resistance [22,25] (see Table 1 for details). Furthermore, we note that a simple masking method was applied for this sample and 6.8% and 93.2% areas of the resultant wafer were textured by MACE and alkaline solution, respectively (see experimental details). It can be anticipated that the cell conversion efficiency will be further improved by optimization of the texturing and mask processes.

4. Conclusions

The surface structures of mono-like Si wafers resultant from different texturing processes correlate with the optical and electrical properties of the solar cells, and the EQE and IQE of the multi-crystalline region are lower than those of the mono-crystalline region, regardless of the different texturing processes. The conversion efficiencies of the solar cells constructed by Si wafers textured by alkaline solution and MACE are 21.37% and 20.99%, respectively, and the combination of these two texturing processes promotes the conversion efficiency to 21.39%. The results suggest that optimizing the surface texturing process and mask method may further improve the efficiency of mono-like Si solar cell.

Credit author statement

Rui Tong: Conceptualization, Methodology, Investigation, Data curation, Writing - original draft. **Weipeng Zhang:** Data curation, Software. **Ximan Ke:** Investigation, Data curation. **Dongming Liu:** Supervision, Conceptualization, Writing - review & editing. **Zhongwei Zhang:** Conceptualization, Resources.

Declaration of competing interest

The authors declare that they have no known competing financial interests or personal relationships that could have appeared to influence the work reported in this paper.

Acknowledgements

This work was supported by the National Natural Science Foundation of China (No. U1503192).

References

- [1] E. Placzek-Popko, Top PV market solar cells 2016, Opto-Electron. Rev. 2 (2017) 55–64, <https://doi.org/10.1016/j.opelre.2017.03.002>.
- [2] H.C. Sio, S.P. Phang, A. Fell, H. Wang, P. Zheng, D.K. Chen, et al., The electrical properties of high performance multicrystalline silicon and mono-like silicon: material limitations and cell potential, Sol. Energy Mater. Sol. Cells 201 (2019), 110059, <https://doi.org/10.1016/j.solmat.2019.110059>.
- [3] L. Gong, F. Wang, Q. Cai, D. You, B. Dai, Characterization of defects in mono-like silicon wafers and their effects on solar cell efficiency, Sol. Energy Mater. Sol. Cells 120 (2014) 289–294, <https://doi.org/10.1016/j.solmat.2013.09.020>.
- [4] Y.C. Wu, A. Lan, C.F. Yang, C.W. Hsu, C.M. Lu, A. Yang, et al., Effect of seed arrangements on the quality of n-type monolike silicon grown by directional solidification, Cryst. Growth Des. 11 (2016) 6641–6647, <https://doi.org/10.1021/acs.cgd.6b01317>.
- [5] C.Y. Lan, Y.C. Wu, A. Lan, C.F. Yang, C. Hsu, C.M. Lu, et al., Control of ingot quality and solar cell appearance of cast mono-like silicon by using seed partitions, J. Cryst. Growth 475 (2017) 136–143, <https://doi.org/10.1016/j.jcrysgr.2017.06.014>.
- [6] K. Dadizis, H. Behnken, T. Bähr, D. Oriwol, L. Sylla, T. Richter, Numerical simulation of stresses and dislocations in quasi-mono silicon, J. Cryst. Growth 450 (2016) 14–21, <https://doi.org/10.1016/j.jcrysgr.2016.06.007>.
- [7] F. Wolny, A. Krause, M. Müller, G. Fischer, H. Neuhaus, Reduced metal contamination from crucible and coating using a silicon nitride based diffusion barrier for the growth of cast quasi-single crystalline silicon ingots, J. Cryst. Growth 514 (2019) 49–53, <https://doi.org/10.1016/j.jcrysgr.2019.02.055>.
- [8] Y. Lv, Y.F. Zhuang, W.J. Wang, W.W. Wei, J. Sheng, S. Zhang, et al., Towards high-efficiency industrial p-type mono-like Si PERC solar cells, Sol. Energy Mater. Sol. Cells 204 (2020), 110202, <https://doi.org/10.1016/j.solmat.2019.110202>.
- [9] C. Liu, D. Chen, Y. Chen, Y. Ling, Y. Zou, Y. Wang, et al., Industrial TOPCon solar cells on n-type quasi-mono Si wafers with efficiencies above 23%, Sol. Energy Mater. Sol. Cells 215 (2020), 110690 <https://doi.org/10.1016/j.solmat.2020.110690>.
- [10] S. Sivasubramaniam, M.M. Alkaissi, Inverted nanopyramid texturing for silicon solar cells using interference lithography, Microelectron. Eng. 119 (2014) 146–150, <https://doi.org/10.1016/j.mee.2014.04.004>.
- [11] J. Wu, Y. Liu, W. Chen, Y. Zhao, Q. Chen, H. Tang, et al., Influence of different-sized inverted-pyramids of silicon texture by Ag manipulation on solar cell performance, Appl. Surf. Sci. 506 (2020), 144778, <https://doi.org/10.1016/j.apsusc.2019.144778>.
- [12] B. Radfar, F. Es, R. Turan, Effects of different laser modified surface morphologies and post-texturing cleanings on c-Si solar cell performance, Renew. Energy 145 (2020) 2707–2714, <https://doi.org/10.1016/j.renene.2019.08.031>.
- [13] J. Yoo, K.-M. Han, J.-S. Cho, Solar cell fabrication using two-step textured quasi-single crystalline silicon by alkaline and RIE texturing processes, Vacuum 128 (2016) 118–122, <https://doi.org/10.1016/j.vacuum.2016.03.023>.
- [14] K. Kim, S.K. Dhungel, S. Jung, D. Mangalaraj, J. Yi, Texturing of large area multi-crystalline silicon wafers through different chemical approaches for solar cell fabrication, Sol. Energy Mater. Sol. Cells 92 (2008) 960–968, <https://doi.org/10.1016/j.solmat.2008.02.036>.
- [15] H. Liu, L. Zhao, H. Diao, W. Wang, High-performance texturization of multicrystalline silicon wafer by HF/HNO₃/H₂O system incorporated with MnO₂ particles, Mater. Sci. Semicond. Process. 101 (2019) 149–155, <https://doi.org/10.1016/j.mssp.2019.06.003>.
- [16] X. Yang, W. Zhang, J. Choi, H.Q. Ta, Y. Bai, L. Chen, et al., Influence of bowl-like nanostructures on the efficiency and module power of black silicon solar cells, Sol. Energy 189 (2019) 67–73, <https://doi.org/10.1016/j.solener.2019.07.044>.
- [17] K. Chen, J. Zha, F. Hu, X. Ye, S. Zou, V. Vähännissi, et al., MACE nano-texture process applicable for both single- and multi-crystalline diamond-wire sawn Si solar cells, Sol. Energy Mater. Sol. Cells 191 (2019) 1–8, <https://doi.org/10.1016/j.solmat.2018.10.015>.
- [18] U. Gangopadhyay, K.H. Kim, S.K. Dhungel, U. Manna, P.K. Basu, M. Banerjee, et al., A novel low cost texturization method for large area commercial mono-crystalline silicon solar cells, Sol. Energy Mater. Sol. Cells 90 (2006) 3557–3567, <https://doi.org/10.1016/j.solmat.2006.06.044>.
- [19] K. Gao, Y. Liu, Y. Fan, L. Shi, Y. Zhuang, Y. Cui, et al., High-efficiency silicon inverted pyramid-based passivated emitter and rear cells, Nanoscale Res. Lett. 15 (2020) 174, <https://doi.org/10.1186/s11671-020-03404-y>.
- [20] H. Kim, S. Park, B. Kang, S. Kim, S.J. Tark, D. Kim, et al., Effect of texturing process involving saw-damage etching on crystalline silicon solar cells, Appl. Surf. Sci. 284 (2013) 133–137, <https://doi.org/10.1016/j.apsusc.2013.07.051>.

- [21] X. Li, Z. Gao, D. Zhang, K. Tao, R. Jia, S. Jiang, et al., High-efficiency multi-crystalline black silicon solar cells achieved by additive assisted Ag-MACE, *Sol. Energy* 195 (2020) 176–184, <https://doi.org/10.1016/j.solener.2019.11.045>.
- [22] X. Dai, R. Jia, G. Su, H. Sun, K. Tao, C. Zhang, et al., The influence of surface structure on diffusion and passivation in multicrystalline silicon solar cells textured by metal assisted chemical etching (MACE) method, *Sol. Energy Mater. Sol. Cells* 186 (2018) 42–49, <https://doi.org/10.1016/j.solmat.2018.06.011>.
- [23] M. Cui, C. Jin, Y. Yang, X. Wu, L. Zhuge, Emitter doping profiles optimization and correlation with metal contact of multi-crystalline silicon solar cells, *Optik* 127 (2016) 11230–11234, <https://doi.org/10.1016/j.ijleo.2016.08.120>.
- [24] A. Safiei, H. Windgassen, K. Wolter, H. Kurza, Emitter profile tailoring to contact homogeneous high sheet resistance emitter, *Energy Procedia* 27 (2012) 432–437, <https://doi.org/10.1016/j.egypro.2012.07.089>.
- [25] E. Kobayashi, S.D. Wolf, J. Levrat, A. Descoedres, M. Despeisse, F.-J. Haug, et al., Increasing the efficiency of silicon heterojunction solar cells and modules by light soaking, *Sol. Energy Mater. Sol. Cells* 173 (2017) 43–49, <https://doi.org/10.1016/j.solmat.2017.06.023>.